arXiv:1612.05069v1 [cond-mat.quant-gas] 15 Dec 2016

Stationary through-flows in a Bose-Einstein condensate with a $\mathcal{PT}$-symmetric impurity

Dmitry A. Zezyulin[1], I. V. Barashenkov[2,3,4], and Vladimir V. Konotop[1]
[1] *Centro de Física Teórica e Computacional and Departamento de Física, Universidade de Lisboa, Campo Grande 2, Edifício C8, Lisboa 1749-016, Portugal*
[2] *Department of Mathematics, University of Cape Town, Rondebosch 7701, South Africa*
[3] *Joint Institute for Nuclear Research, Dubna 141980, Russia*
[4] *Department of Physics, University of Bath, Claverton Down, Bath BA2 7AY, UK*
(Dated: December 16, 2016)

Superfluid currents in the boson condensate with a source and sink of particles are modelled by the $\mathcal{PT}$-symmetric Gross-Pitaevskii equation with a complex potential. We demonstrate the existence of through-flows of the condensate — stationary states with the asymptotically nonvanishing flux. The through-flows come in two broad varieties determined by the form of their number density distribution. One variety is described by dip-like solutions featuring a localised density depression; the other one comprises hump-like structures with a density spike in their core. We exemplify each class by exact closed-form solutions. For a fixed set of parameters of the $\mathcal{PT}$-symmetric potential, stationary through-flows form continuous families parametrized by the strength of the background flux. All hump-like and some dip-like members of the family are found to be stable. We show that the through-flows can be controlled by varying the gain-and-loss amplitude of the complex potential and that these amplitude variations may produce an anomalous response of the flux across the gain-loss interface.

PACS numbers: 03.75.Lm, 42.65.Tg

I. INTRODUCTION

An important macroscopic property of degenerate quantum gases is their ability to conduct superfluid currents. The superfluid flows in atomic Bose-Einstein condensates (BECs) have been thoroughly analysed in a variety of settings characterised by real and complex external potentials [1]. The conservative systems modelled by the real potentials comprised linear [2] and nonlinear [3] optical lattices, localised impurities [4], and potential barriers [5]. The superfluid currents in localised dissipative potentials were also studied in atomic BECs, theoretically [6] and experimentally [7], with the macroscopic Zeno effect [8] being observed. The corresponding physical contexts included also the exciton-polariton condensates [9].

In this paper, we consider hydrodynamic currents in a general nonconservative model with a complex potential [10]. Specifically, we are interested in parity-time ($\mathcal{PT}$-) symmetric arrangements. The importance of the $\mathcal{PT}$ symmetry for different branches of physics has been widely appreciated [11] since it was introduced in the non-Hermitian quantum mechanics [12]. The quantum $\mathcal{PT}$-symmetric systems are defined by non-Hermitian Hamiltonians commuting with the composition of the space and time inversion. Non-Hermitian $\mathcal{PT}$-symmetric Hamiltonians may have all-real spectra in certain parameter domains.

The similarity between the Schrödinger equation of quantum mechanics and the mean-field Gross-Pitaevskii equation inspired studies of BECs in the presence of $\mathcal{PT}$-symmetric potentials [11, 13]. Nontrivial flows in a $\mathcal{PT}$-symmetric condensate may result from the balance of the particle influx and leakage. The persistent currents in $\mathcal{PT}$-symmetric atomic condensates have been considered primarily in the tight-binding approximation [14]. This approximation reduces the rich wave dynamics of the Gross-Pitaevskii equation to the interaction of just a few modes. As for the currents in the full infinite-dimensional $\mathcal{PT}$-symmetric system, these have been discussed only recently, in connection with the jamming anomaly [15] and nonlinear flows supported by pseudo-spectral singularities in a ring-shaped waveguide [16]. (The jamming anomaly consists in the drop of the flux from the pumped to the leaking site despite their common gain and loss amplitude being raised. It is a relative of the macroscopic Zeno effect [6–8] understood as the attenuation of the condensate depletion as the atom removal rate is increased at the removal sites.)

The paper [15] focussed on localised stationary states, with all fluxes assumed to be vanishing at infinity. As that earlier analysis, the present study deals with stationary currents in the Gross-Pitaevskii equation with a localised complex potential in the form of a $\mathcal{PT}$-symmetric dipole. In difference to Ref. [15], we consider the situation where in addition to the flux generated by the dipole, there are nonvanishing background fluxes — that is, currents originating at one infinity and running toward the other one. We show that the balance of the nonlinearity, dispersion and Hermitian well-shaped potential, with the assistance of the local flux generated by the gain-loss dipole, produces stable localised structures in the condensate of constant density flowing at a constant speed. The presence of gain and loss may give rise to highly nontrivial spatial profiles of the superfluid current. In particular, we report stable stationary structures consisting of a finite-size patch of current embedded in the background flow of opposite direction.

The outline of the paper is as follows. In the next

section, the problem of stationary flows in the condensate with gain and loss is formulated as a stationary $\mathcal{PT}$-symmetric Gross-Pitaevskii equation with nonvanishing boundary conditions. In Sec. III we establish the existence of the through-flow currents in a special type of $\mathcal{PT}$-symmetric potential, the so-called Wadati potential. The structure of the Wadati potential allows to obtain the solution of the associated Gross-Pitaevskii equation in closed form.

Section IV looks into stationary through-flows in generic $\mathcal{PT}$-symmetric potentials outside the Wadati variety. A potential with a fixed set of parameters is shown to support a continuous family of through-flow solutions that can be parametrised by the asymptotic flux and background density. Part of the family have a density dip and the other part density spike in their core. Section V examines stability of the through-flows. In section VI we explore the response of the interfacial flux associated with the stationary through-flows, to the variation of the gain-loss coefficient. Finally, section VII summarises conclusions of this study.

II. STATIONARY THROUGH-FLOWS

We consider the dimensionless Gross-Pitaevskii equation

$$i\Psi_t = -\Psi_{xx} + U(x)\Psi + 2|\Psi|^2\Psi, \tag{1}$$

with a decaying potential $U(x) \to 0$ as $|x| \to \infty$. The potential satisfies $U(x) = U^*(-x)$ and has the nature of a $\mathcal{PT}$-symmetric defect. The sign of $\mathrm{Im}\, U(x)$ determines whether the particles are fed into the system (this is the situation in the region with $\mathrm{Im}\, U > 0$) or eliminated from the condensate (the corresponding domain is characterised by $\mathrm{Im}\, U < 0$). The nonlinearity in (1) corresponds to the two-body repulsion between bosons.

The quantity

$$n(x,t) = |\Psi|^2$$

gives the density of the number of particles in the condensate,

$$J(x,t) = i(\Psi_x^*\Psi - \Psi^*\Psi_x)$$

is the associated flux, and

$$v(x,t) = \frac{J}{n}$$

is the superfluid velocity.

The aim of this paper is to study nonlinear structures induced by a localized $\mathcal{PT}$ symmetric potential $U(x)$ in nonzero superfluid flows. Accordingly, we impose the boundary conditions in the form

$$\lim_{x\to\pm\infty} n(x,t) = n_\infty, \tag{2a}$$

$$\lim_{x\to\pm\infty} J(x,t) = J_\infty, \tag{2b}$$

where the background density $n_\infty \neq 0$ and flux $J_\infty \neq 0$. Solutions representing stationary flows have the form $\Psi(x,t) = e^{-i\mu t}\psi(x)$, where μ is the chemical potential. The spatial part of the solution solves the equation

$$-\psi_{xx} + U(x)\psi + 2\psi|\psi|^2 = \mu\psi. \tag{3}$$

In the stationary regime the number density, flux and superfluid velocity are time-independent: $n = n(x)$, $J = J(x)$, and $v = v(x)$.

The stationary configurations of condensate with equal nonvanishing inflow and outflow of particles, will be referred to as the *through-flows* in what follows.

The absolute value of the background flux is uniquely determined by the chemical potential and background density. Making use of the boundary conditions (2) as well as the fact that $U(x) \to 0$, equation (3) gives

$$\left(\frac{J_\infty}{2n_\infty}\right)^2 = \mu - 2n_\infty. \tag{4}$$

We also note that for the given background density n_∞ (and varying chemical potential), the background flux cannot exceed a certain finite limit. Linearising equation (3) with $U = 0$ about the asymptotic solution $\psi = \sqrt{n_\infty}e^{i(\nu/2)x}$, where

$$\nu = \frac{J_\infty}{n_\infty}, \tag{5}$$

the small perturbation is found to have the form

$$\delta\psi(x) = e^{i(\nu/2)x}\left[(A+iB)e^{-2\kappa x} + (A^*+iB^*)e^{-2\kappa^* x}\right],$$

where A and B are complex constants. The decay rate 2κ satisfies

$$\kappa^2\left[\kappa^2 - \left(n_\infty - \frac{\nu^2}{4}\right)\right] = 0.$$

Perturbations $\delta\psi$ that decay as $x \to \infty$ have

$$\kappa^2 = n_\infty - \frac{\nu^2}{4} > 0.$$

Substituting (5) in $\nu^2 < 4n_\infty$ gives

$$|J_\infty| \leq 2\sqrt{n_\infty^3}. \tag{6}$$

We will be mindful of this simple bound when considering the variation of the background current J_∞ (section IV).

Our final remark here is that solutions with nonvanishing condensate density at infinity may only arise if $\mu > 0$. This is an obvious consequence of equation (4).

III. WADATI POTENTIALS AND EXACT SOLUTIONS

A simple way to demonstrate the existence of stationary $\mathcal{PT}$-symmetric through-flows and illustrate their

properties, is to produce an explicit solution. To this end, we consider a $\mathcal{PT}$-symmetric potential of the special form

$$U(x) = -w^2(x) + iw_x(x), \tag{7}$$

where $w(x)$ is an even real-valued function (referred to as the *base* function in what follows).

Wadati [17] was the one who has originally noted rich $\mathcal{PT}$-symmetric properties of potentials of this form. The existence of localized nonlinear modes supported by potentials (7) was established in [18, 19]. Ref. [20] studied the symmetry breaking while Ref. [21] explored the modulation instability of a constant-density solutions arising in the Wadati potentials. More complicated closed-form solutions in Wadati potentials were found in [22]. In the present work, we exploit the analytical tractability of these potentials to derive an exact solution describing a stationary through-flow with a spatially localized rarefaction or compression.

A. Two-parameter Wadati family

To facilitate the analysis of the flux profile associated with a through-flow, we try to keep the corresponding density distribution simple. Specifically, we take

$$n = \frac{\mu}{2}\left(1 + a\,\mathrm{sech}^2 y\right), \quad y = x\sqrt{\mu/2}\sin\phi. \tag{8}$$

The density (8) is characterised by two parameters that can be freely chosen in the following ranges:

$$a > -1, \quad 0 \le \phi \le \pi/2. \tag{9}$$

Negative values of a ($-1 < a < 0$) correspond to densities with a dip at the origin and positive a to hump-shaped distributions. The angle ϕ determines the characteristic width of the dip or hump.

The Wadati potential (7) supporting the solution with the density (8), is generated by the base function

$$w = -\frac{\sqrt{2\mu}}{4}\frac{2\cos^2\phi\cosh^2 y + 3(a+\sin^2\phi)}{\cosh y\sqrt{\cosh^2 y\cos^2\phi + a + \sin^2\phi}}. \tag{10}$$

(See the Appendix for the derivation.) The superfluid velocity $v = 2\theta_x$ associated with the density (8) and potential (7)+(10), has the form

$$v = -\frac{\sqrt{2\mu}}{2}\frac{\mathcal{N}}{\mathcal{D}}, \tag{11}$$

with

$$\mathcal{N} = 2\cos^2\phi\cosh^4 y + (a+\sin^2\phi)(a+3\cosh^2 y)$$

and

$$\mathcal{D} = \cosh y\left(a+\cosh^2 y\right)\sqrt{\cosh^2 y\cos^2\phi + a + \sin^2\phi}.$$

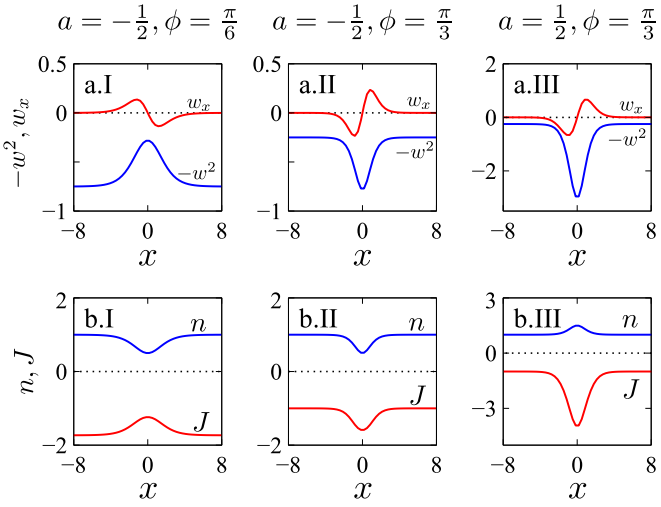

FIG. 1: The Wadati potentials (7), (10) (top row) and the corresponding exact solutions (8), (11) (bottom row). The left column (column I) corresponds to $a = -1/2$, $\phi = \pi/6$; the middle column (II) to $a = -1/2$, $\phi = \pi/3$, and the right column (III) to $a = 1/2$, $\phi = \pi/3$. The three columns exemplify potentials and solutions at the points I, II, and III in Fig. 2. In the top row, the blue and red lines depict the real and imaginary parts of the potential (7), (10). In the bottom row, the blue curves describe the number density and the red ones show the flux J associated with the solution (8), (11). In these plots, $\mu = 2$.

The imaginary part of the Wadati potential with the base (10) is given by

$$w_x = (a + \sin^2\phi)\tanh y\,\mathcal{W}(y). \tag{12}$$

Here

$$\mathcal{W}(y) = \frac{\mu\sin\phi\left[4\cos^2\phi\cosh^2 y + 3(a+\sin^2\phi)\right]}{4\cosh y\left(\cos^2\phi\cosh^2 y + a + \sin^2\phi\right)^{3/2}}$$

is an even function; it is not difficult to verify that $\mathcal{W}(y) > 0$. Hence the derivative (12) is positive in one x-semiaxis and negative in the other. This arrangement corresponds to a $\mathcal{PT}$-symmetric dipole: the particles are gained in one half of the x-line and lost in the other one.

Note that the "polarity" of the dipole switches around as the sign of the sum $a + \sin^2\phi$ is changed. When $a + \sin^2\phi < 0$, the particles are gained in the left semi-axis and lost in the right one, whereas when $a + \sin^2\phi > 0$, the region of gain is to the right of the region of loss.

The real and imaginary parts of the resulting potential U are exemplified in Fig. 1, in the top row. The condensate density (8) and flux $J = vn$ with v as in (11), are shown in the bottom row of Fig. 1.

Although the potential $U(x)$ does not decay to zero as $|x| \to \infty$, it has finite and equal asymptotic values $U(\pm\infty) = U_\infty < 0$. Accordingly, the "uplifted" potential $\widetilde{U}(x) = U(x) - U_\infty$ does decay to zero and the analysis of the previous section remains valid if we replace μ with $\widetilde{\mu} = \mu - U_\infty$.

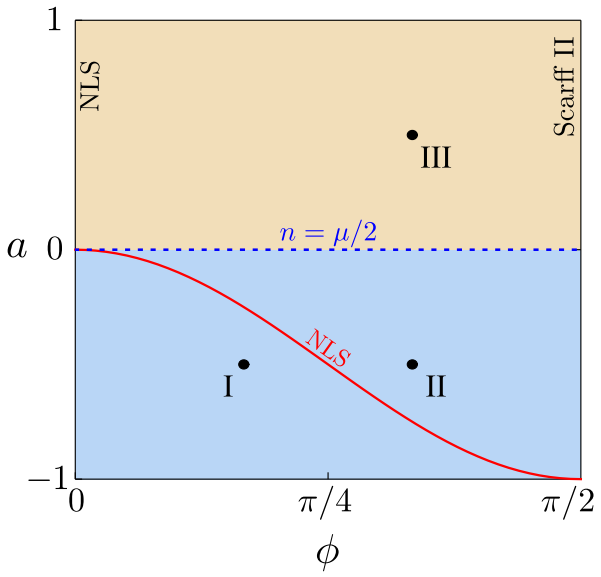

FIG. 2: (Color online) The parameter plane for the Wadati potential (7), (10) and the corresponding solution (8), (11). In the regions I and II (coloured blue) the solution has the form of a dip in a constant density — see panels (b.I) and (b.II) of Fig.1. In the domain demarcated by III (tinted brown), the soliton is hump-like — see panel (b.III) of Fig.1. Note that the domain III does not have an upper bound and extends indefinitely in a. The red curve separating domains I and II is given by $a = -\sin^2\phi$. Along this curve and along the vertical line $\phi = 0$, the potential is real and the through-flow reduces to the nonlinear Schrödinger (NLS) dark soliton. Along the other boundary, $\phi = \pi/2$, the potential is the $\mathcal{PT}$-symmetric Scarff II.

Computing the superfluid current for the solution (8), (11), we arrive at

$$J_\infty = -\sqrt{\frac{\mu^3}{2}}\cos\phi. \tag{13}$$

The background flux is negative for all ϕ between 0 and $\pi/2$. This implies that the condensate flows in the negative direction on the x-line — irrespective of the choice of μ, a, and ϕ. The direction of the asymptotic current is unaffected even when the sign of $a + \sin^2\phi$ is changed so that the local gain and loss sites are swopped around. This is clearly visible in panels I and II of Fig. 1. [The invariance of the current direction does not mean that there are no through-flows with positive asymptotic flux though. The positive through-flows result from expressions (A17) in the Appendix. Those have $n(x)$ as in (8) but $w(x)$ and $v(x)$ opposite to the expressions in (10) and (11).]

The density and velocity fields being time-independent, the solution (8), (11) represents a stationary mode pinned on a localised defect. In the frame of reference moving with the negative velocity $\nu = J_\infty/n_\infty$, the mode and defect appear to travel at a constant positive velocity $-\nu$. The inequality (6) amounts to $-\nu < c$, where c is the speed of sound in the frame of the flow: $c = 2\sqrt{n_\infty}$. This explains the absence of any Cherenkov radiations excited by the moving defect.

Using equations (8) and (11), we obtain the flux at the point $x = 0$ separating the active from the lossy region:

$$J(0) = -\sqrt{\frac{\mu^3(a+1)}{8}}(a + \sin^2\phi + 2). \tag{14}$$

The flux across the gain-loss interface is negative — regardless of the choice of μ, a, and ϕ. When the potential parameters satisfy $a+\sin^2\phi < 0$, the flux negativity could seem to contradict the fact that particles are gained to the left and lost to the right of the origin.

To resolve this "paradox" we notice that

$$J(0) = -2\int_0^\infty |\psi|^2\,\mathrm{Im}\,U(x)\,dx + J_\infty. \tag{15}$$

The first term on the right accounts for the gain or loss of particles in the region $x > 0$. Despite this term being positive for $a + \sin^2\phi < 0$, the flux $J(0)$ ends up being negative due to the second, negative, term. The fact that $J(0) < 0$ implies simply that the background flux J_∞ is greater, in absolute value, than the gain or loss rate in the finite part of the system.

B. Four special cases

The solution (8), (11) and the underlying potential (7), (10) include several particular cases that are relevant in the context of recent studies. The corresponding parameter pairs are marked in the parameter plane of Fig.2.

First, letting $a = 0$ produces a solution of uniform density:

$$\psi(x) = \sqrt{\frac{\mu}{2}}\exp\left\{i\int w(x)dx\right\}.$$

The modulation instability of a solution of this sort was studied in the equation with a periodic potential [21].

Second, equations (7) and (10) with $\phi = \pi/2$ amount to the familiar $\mathcal{PT}$-symmetric Scarff II potential [23]. The corresponding base function is given by

$$w(x) = -\frac{3\sqrt{2}\mu}{4}\sqrt{1+a}\,\mathrm{sech}\,y. \tag{16}$$

Solutions of the repulsive nonlinear Schrödinger equation with the $\mathcal{PT}$-symmetric Scarff II potential and vanishing boundary conditions, have been studied in [24]. Our solution (8), (11) with $\phi = \pi/2$ is different from those localized modes. It represents a dip (for $-1 < a < 0$) or a hump (for $a > 0$) over a nonzero background (with an asymptotically vanishing flux).

Third, the choice $a = -\sin^2\phi$ corresponds to the spatially-homogeneous conservative situation. In this

particular case, the base function reduces to a constant,

$$w(x) \equiv w_0, \quad w_0 = -\sqrt{\frac{\mu}{2}}\cos\phi, \tag{17}$$

so that the real part of the potential $U(x)$ becomes constant and the imaginary part zero. The solution (8), (11) becomes the dark soliton of the repulsive nonlinear Schrödinger equation.

The role of the curve $a = -\sin^2\phi$ on the parameter plane of Fig.2 can be appreciated by evaluating the difference between the interfacial and background flux for the solution (8), (11). We have

$$|J(0)| - |J_\infty| = (a + \sin^2\phi)\mathcal{Q}, \tag{18}$$

where

$$\mathcal{Q} = \frac{\mu^{3/2}}{2\sqrt{2}} \frac{\sqrt{a+1}\cos\phi + a + 3}{\sqrt{a+1} + \cos\phi} > 0.$$

In the region I (region below the curve), the interfacial flux is smaller than the background flux in absolute value, while in the region II (above the curve), the difference (18) is positive. [Compare panels (b.I) and (b.II) of Fig.1.]

This change of sign is a natural consequence of equation (15) which relates the difference (18) to the loss rate in the right semiaxis. Crossing the curve $a = -\sin^2\phi$ switches the gain and loss around — see the expression (12) for the imaginary part of the Wadati potential. At points lying on the curve, the system does not experience any gain or loss; hence the current is spatially uniform. In particular, $J(0) = J_\infty$.

The fourth simple particular case is defined by $\phi = 0$. As in the previous situation, the base function is a constant here:

$$w = -\frac{\sqrt{2\mu}}{4}\frac{2+3a}{\sqrt{1+a}}.$$

Hence the $\phi = 0$ limit also corresponds to the homogeneous conservative nonlinear Schrödinger equation. In this case, equations (8), (11) give an x-independent solution:

$$n = \frac{\mu}{2}(1+a), \quad v = -\frac{\sqrt{2\mu}(a+2)}{2\sqrt{a+1}}. \tag{19}$$

IV. CONTINUOUS FAMILIES

Like solitons in conservative systems, localised modes (solutions decaying to zero at infinities) in nonlinear $\mathcal{PT}$-symmetric equations form a continuous family for each set of parameter values of the model (see reviews [11, 25]). The aim of this section is to show that the stationary $\mathcal{PT}$-symmetric through-flows share this property. Namely, a fixed $\mathcal{PT}$-symmetric potential supports a family of through-flows parametrised by the background number density and flux.

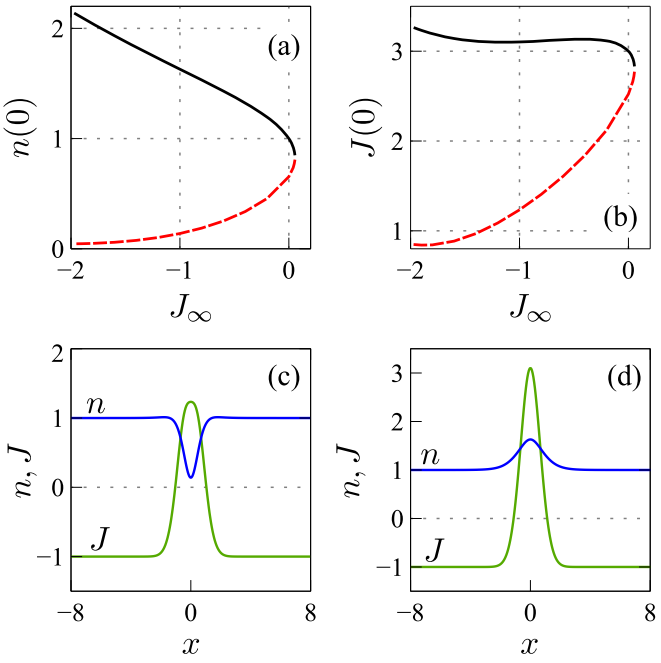

FIG. 3: A family of through-flows supported by the $\mathcal{PT}$-symmetric Gaussian potential (20) with $\gamma = 3/2$ and $U_0 = 9/4$. The left panel traces $n(0)$ as J_∞ is varied, and the right panel displays the corresponding $J(0)$. Solid (black) and dashed (red) segments of curves correspond to stable and unstable solutions, respectively. The bottom panels show examples of a dip (c) and a hump (d) pertaining to $J_\infty = -1$. The blue line depicts $n(x)$ and the green one shows $J(x)$. In all panels, the background density is set to $n_\infty = 1$; the largest value of $|J_\infty|$ attainable by this family is determined by equation (6): $J_\infty = -2$. The starting point of continuation is the top point with $J_\infty = 0$; here $n(0)$ and $J(0)$ are determined by the exact solution (21): $n(0) = 1$ and $J(0) = 3$.

We demonstrate the existence of continuous families of through-flows by considering a simple $\mathcal{PT}$-symmetric potential in the form of a Gaussian potential well:

$$U(x) = -U_0\exp(-2x^2) - 2i\gamma x\exp(-x^2). \tag{20}$$

Here $U_0 > 0$ is the depth of the well and γ is commonly referred to as the gain-loss coefficient, or the gain-loss amplitude. A positive γ corresponds to the dissipative domain being placed to the right of the origin and the active region being on its left. For negative γ the arrangement is reversed: particles are lost in the left and gained in the right semiaxis.

Keeping U_0, γ, and the background density n_∞ fixed, we continue the solution $\psi(x)$ in μ numerically. The background flux J_∞ is related to μ by equation (4); it is instructive to use J_∞ as the parameter of the family.

Note that when $U_0 = \gamma^2$, the gaussian potential (20) belongs to the Wadati variety (7), with $w(x) = \gamma e^{-x^2}$. In this case, equation (3) admits [21] an exact uniform-

density solution

$$\psi(x) = \exp\left\{\frac{i\sqrt{\pi}\gamma}{2}\,\mathrm{erf}\,(x)\right\}. \tag{21}$$

The background flux associated with the solution (21), vanishes: $J_\infty = 0$. Equation (4) gives the corresponding chemical potential: $\mu = 2n_\infty$. We use the above solution as a starting point for our numerical continuation.

A typical one-parameter family is traced in Fig. 3(a,b). In the left panel of that figure, each through-flow is represented by the density of the condensate at the origin. In the right panel, we employ the interfacial flux as an alternative bifurcation measure.

Each bifurcation curve consists of two branches separated by a turning point. Solutions on the whole of the red (dashed) branch and on a short section of the black (solid) branch characterised by positive J_∞, have the form of a dip in the uniform background: $n(0) < n_\infty$. Solutions on the remaining part of the black branch ($J_\infty < 0$) represent humps: $n(0) > n_\infty$. The largest attainable value of $|J_\infty|$ in Fig. 3(a,b) is set by the bound (6).

The dips and humps are exemplified by Fig. 3(c,d). The density $n(x)$ and the superfluid flux $J(x)$ have the form similar to that of the dips and humps borne by the Wadati potentials of the previous sections [cf. Fig. 1(b)]. The "flat" solution (21) serves as a watershed between the two classes of through-flows.

For the most part of the bifurcation curve in Fig. 3(b), the background and interfacial flux have opposite signs. [This is at variance with the through-flow (8), (11) supported by the Wadati potential (7)+(10).] Therefore, each through-flow consists of a patch of positive current embedded in the negative background flow. Equation (15) and the inequality $J(0)J_\infty < 0$ imply that the background flux J_∞ is smaller in absolute value than the total loss rate in the domain where atoms are removed, $x > 0$. (The same applies to the total gain rate in the domain where atoms are loaded, $x < 0$.) In other words, the gain and loss corresponding to the chosen parameters of the potential are intense enough to reverse the background flow locally. Turning the background flux J_∞ up continuously from negative to positive values does not change the direction of the interfacial current, so the above inequality is replaced with $J(0)J_\infty > 0$. However this relation appears to be unsustainable over an extended interval of J_∞-values and the branch is forced to turn back soon after the background flux has changed its sign.

V. STABLE HUMPS UNSTABLE DIPS

To examine the stability of dips and humps, we let

$$\Psi = \left[\psi + (f + ig)e^{\lambda t}\right] e^{-i\mu t},$$

where $\psi(x)$ is the solution whose stability is analysed, and $f(x) + ig(x)$ is a small perturbation. Substituting in (1) and linearising in f and g, we arrive at an eigenvalue problem

$$\mathcal{H}\vec{y} = \lambda\mathcal{J}\vec{y}, \tag{22}$$

where

$$\mathcal{H} = \begin{pmatrix} \mathcal{L} + 6p^2 + 2q^2 & -\mathrm{Im}\,U(x) + 4pq \\ \mathrm{Im}\,U(x) - 4pq & \mathcal{L} + 2p^2 + 6q^2 \end{pmatrix},$$

$$\mathcal{L} = -\frac{d^2}{dx^2} - \mu + \mathrm{Re}\,U(x),$$

$$\vec{y} = \begin{pmatrix} f \\ g \end{pmatrix}, \quad \mathcal{J} = \begin{pmatrix} 0 & -1 \\ 1 & 0 \end{pmatrix}$$

and we have decomposed

$$\psi(x) = p(x) + iq(x).$$

The solution $\psi(x)$ is deemed unstable if there is at least one eigenvalue with $\mathrm{Re}\,\lambda > 0$.

The eigenvalue problem (22) was analysed numerically. The dip-like solutions on the red branch in Fig. 3 were found to be all unstable. On the other hand, the black branch consists of stable through-flows. This branch includes all hump-like solutions and a small segment of dips (the segment with $J_\infty > 0$).

The instability of the dips far from the turning point is due to a quadruplet of complex eigenvalues $(\pm\lambda, \pm\lambda^*)$ and a pair of opposite real eigenvalues. Approaching the turning point along the red curve, the complex eigenvalues converge, pairwise, on the imaginary axis — but the real ones persist. At the turning point, the real pair converges at the origin and moves on to the imaginary axis.

The conclusions of the linear stability analysis have been verified in direct computer simulations of the full time-dependent Gross-Pitaevskii equation (1). Fig. 4 exemplifies the evolution of perturbed hump and dip solutions supported by the potential (20) with the same values of U_0 and γ, and corresponding to the same background flow. A small perturbation of the hump is observed to disperse away leaving the hump intact [Fig. 4 (a,c)]. In contrast, a small perturbation of the linearly unstable dip solution triggers its transformation into the hump with the equal background flux and density [Fig. 4 (b,d)]. The emergent hump persists indefinitely.

VI. VARYING GAIN AND LOSS

In a structureless $\mathcal{PT}$-symmetric dipole system, raising the gain and loss coefficient boosts the flux between its active and dissipative components — hence intensifying the gain and loss in the dimer [15]. In contrast, systems with internal spatial structure modelled by the Gross-Pitaevskii equation may exhibit an anomalous behaviour.

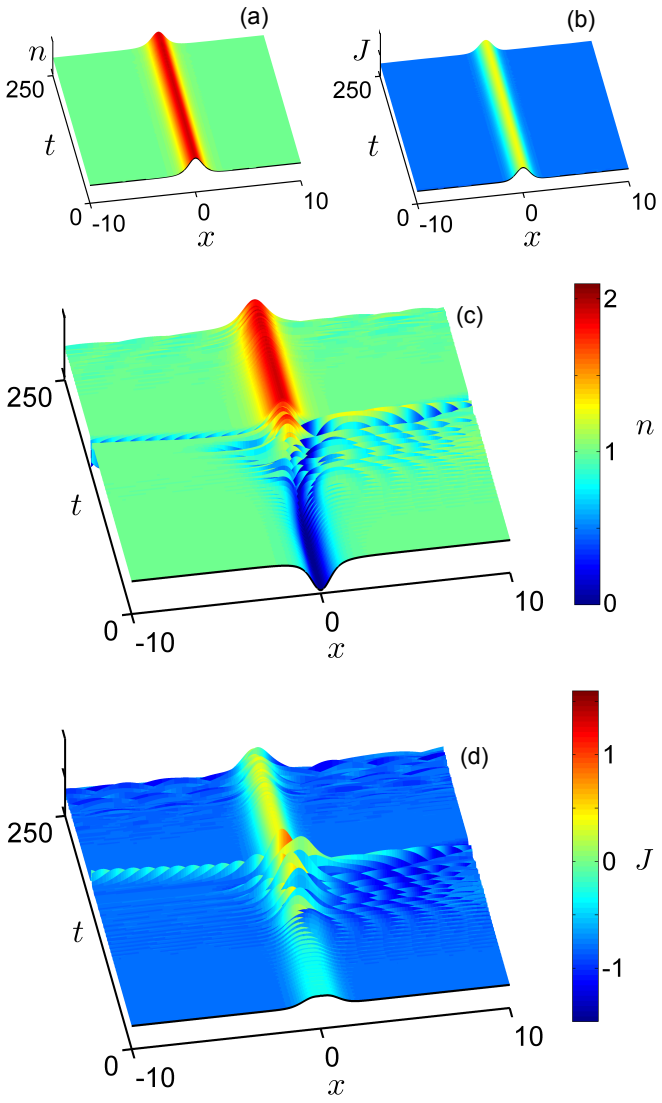

FIG. 4: The evolution of a hump (a,b) and coexisting dip solution (c,d). The panels (a,c) display the density $n(x,t) = |\Psi|^2$, and the panels (b,d) show the flux $J(x,t) = 2(\arg\Psi)_x|\Psi|^2$. The hump solution was initially perturbed by a gaussian-shaped perturbation with an amplitude of 2% of the amplitude of the hump. No explicit perturbation was added to the dip solution initially; here the instability was seeded by the discretisation error. In these plots, $U_0 = 9/4$, $\gamma = 0.4$, $n_\infty = 1$, and $J_\infty = -0.8$.

This *jamming anomaly* manifests itself in the drop of the interfacial flux as a result of the growth of the gain-loss coefficient: $dJ(0)/d\gamma < 0$ [15].

In this section we explore the response of the interfacial flux associated with the stationary through-flows, to the variation of the gain-loss coefficient. For this analysis, we employ the complex potential (20).

Choosing a pair of values for n_∞ and J_∞, with $|J_\infty| \leq 2n_\infty^{3/2}$, fixes a particular member of the family of through-flows. Keeping the potential-well depth U_0 fixed and letting γ to be varied, we determine this solution numerically. In Fig. 5 we represent this through-flow using two scalar characteristics familiar from the previous section: $n(0)$ and $J(0)$.

The transformation $\gamma \to -\gamma$, $x \to -x$ leaves the equation (3) with potential (20) invariant while flipping the sign of the flux J. Accordingly, we restrict ourselves to nonpositive values of J_∞. To recover a solution with $J_\infty > 0$ and, say, $\gamma > 0$, one just needs to reflect a solution with $\gamma < 0$ about the origin on the x-line.

Figure 5 traces the family of solutions with the vanishing background current and another one, corresponding to a negative J_∞. In either case, there are two coexisting through-flows for each value of γ. As indicated by the solid and dashed lines in Fig. 5, all hump-shaped solutions are stable whereas most of the dip-shaped ones are unstable. The loss of stability occurs in the vicinity of the turning point. (It would be tempting to believe that the stability is lost exactly at the turning point; however our numerics suggest that this is not the case, at least for the nonzero asymptotic flux J_∞.)

Away from the turning point, i.e., in the small-$|\gamma|$ region, the unstable dip solution features a quadruplet of complex eigenvalues signalling an oscillatory instability. For larger γ, there also is a pair of opposite real eigenvalues. As γ approaches the turning point, the complex quadruplet converges on the imaginary axis and then the real pair moves on to the imaginary axis as well.

In the absence of the background flux ($J_\infty = 0$), the $n(\gamma)$-curve is symmetric with respect to the n-axis (Fig. 5(a)) and the $J(\gamma)$-curve is symmetric under the $\gamma \to -\gamma, J \to -J$ reflection (Fig. 5(b)). This is an obvious consequence of the $\gamma \to -\gamma$, $x \to -x$ invariance of equation (3). The interfacial flux $J(0)$ is positive if $\gamma > 0$ and negative if $\gamma < 0$. This direction of the current is set by the left-right arrangement of the gain and loss in (20).

The nonzero background flux ($J_\infty < 0$) breaks the symmetries of the diagrams — see Fig. 5(c,d). As a result, an interval of small positive γ appears where $J(0) < 0$. For γ in this interval, the background flux J_∞ is greater, in the absolute value, than the gain or loss rate in the finite part of the system. [A similar situation arises in the Wadati potential (7), (10) with $a + \sin^2\phi < 0$; see the discussion of the associated "paradox" at the end of section III A.]

For γ outside this interval adjacent to the origin, we have $J(0) > 0$ — the gain and loss rates exceed the background flux. It is interesting to note two isolated values of γ, one for the hump and the other for the dip branch, where the interfacial flux vanishes: $J(0) = 0$. At these γ, the background current is exactly compensated by the flux generated by the gain and loss.

The dependence of the interfacial flux on the gain-loss amplitude is nonanomalous: $dJ(0)/d\gamma > 0$, for all γ except small neighbourhoods of the turning points where the flux jamming is observed: $dJ(0)/d\gamma < 0$. [See Fig. 5(b,d).]

The nonmonotonic dependence of the interfacial current on the gain-loss coefficient in Figs. 5(b, d) is a

demonstration of the *macroscopic Zeno effect* [6–8]. Indeed, the descending section of the curve on the $J(0)$ vs γ diagram, with J_∞ being fixed, corresponds to the suppression of the loss of the condensed atoms in the domain where they are removed (increase of number of atoms in the domain where they are loaded) as the intensity of removal (loading) of atoms is increased.

It is worth noting that the domain of existence and stability of the through-flows can be controlled by varying the background flux J_∞. For instance, the existence domain of solutions with $J_\infty = 0$ is bounded from above by the turning point at $\gamma_0 \approx 1.53$ [Fig. 5 (a,b)]. Raising the magnitude of the negative flux J_∞ to 0.8 shifts the turning point γ_0 to approximately 1.95 [Fig. 5 (c,d)]. Thus, sending superfluid current through the system with gain and loss ensures that the condensate exists and remains stable under larger gain and loss amplitudes:

$$\gamma_0\Big|_{J_\infty=-0.8} > \gamma_0\Big|_{J_\infty=0}.$$

Finally, we note that the hump- and dip-like solutions discussed in sections IV-VI are not the only through-flows supported by the $\mathcal{PT}$-symmetric system with background flux. In particular, we were able to detect branches of symmetric double- and triple-dip solutions in addition to the single-dip branch. We do not elaborate on these here since all multi-dip complexes were found to be unstable — like their individual constituents.

VII. CONCLUDING REMARKS

In this paper, we considered superfluid currents in the boson condensate with the symmetrically arranged source and sink of particles. We have demonstrated the existence of the through-flows of the condensate — stationary states with the asymptotically nonvanishing flux. These structures were described by solutions of the $\mathcal{PT}$-symmetric Gross-Pitaevski equation with nonvanishing boundary conditions.

The stationary through-flows were exemplified by explicit solutions associated with the $\mathcal{PT}$-symmetric Wadati potentials. We have shown that the through-flows fall under two broad classes determined by the form of their number density distribution. The dip-like solution features a localised density depression and the hump-like structure has a density spike in its core.

The stationary through-flows supported by a given $\mathcal{PT}$-symmetric potential form a continuous family that can be parametrised by the asymptotic flux and background density. The family includes both dip- and hump-like solutions. All humps have been found to be stable whereas the dip-like solutions are unstable — except for a short interval of stability adjacent to the parameter domain of humps. It is important to emphasise that instability is an inherent property of the dip solutions that persists for any arrangement of gain and loss relative to the direction of the background flux.

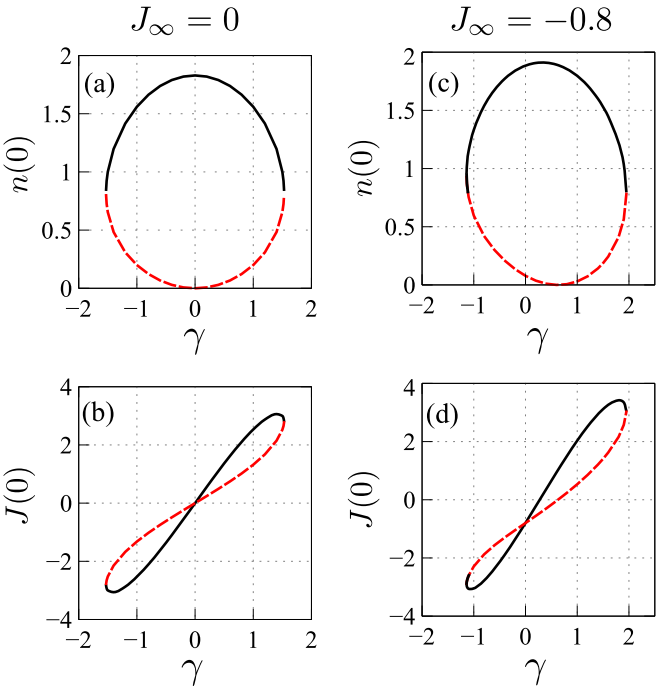

FIG. 5: The density at $x = 0$ and the interfacial flux associated with the through-flows in the Gaussian $\mathcal{PT}$-symmetric potential (20) with $U_0 = 9/4$ and varying γ. Panels (a) and (b) illustrate the case $J_\infty = 0$. Panels (c) and (d) correspond to $J_\infty = -0.8$. Solid lines trace stable through-flows; unstable solutions are marked by dashes. In this figure, $n_\infty = 1$.

We have also explored the response of the interfacial flux associated with the stationary through-flows to the variation of the gain-loss coefficient and described the associated anomalies.

Appendix A: Wadati potential and exact solutions

In this Appendix, we derive the exact solution (8), (11) of the stationary Gross-Pitaevskii equation with the Wadati base function (10).

Following the procedure outlined in [22], we write equation (3) as a first-order system

$$\begin{aligned} \psi_x - iw\psi + \phi = 0, \\ \phi_x + iw\phi + 2\psi|\psi|^2 - \mu\psi = 0. \end{aligned} \tag{A1}$$

The solution $\psi(x)$ and the base function $w(x)$ are constructed in parallel. The procedure is not assuming that $w(x) \to 0$ as $|x| \to \infty$ and accordingly, the Wadati potential (7) does not have to approach zero at the infinities.

Substituting the polar decompositions

$$\psi = \rho e^{i\theta}, \quad \phi = \sigma e^{i\chi}$$

in (A1) gives equations for the moduli and arguments of

$\psi(x)$ and $\phi(x)$:

$$\rho_x + \sigma\cos\alpha = 0, \tag{A2}$$

$$\sigma_x - \rho(\mu - 2\rho^2)\cos\alpha = 0, \tag{A3}$$

$$(\theta_x - w)\rho + \sigma\sin\alpha = 0, \tag{A4}$$

$$(\chi_x + w)\sigma + \rho(\mu - 2\rho^2)\sin\alpha = 0. \tag{A5}$$

Here

$$\alpha = \chi - \theta \quad (0 \le \alpha \le \pi).$$

Eliminating $\cos\alpha$ between (A2) and (A3) we obtain a conservation law [19]

$$\mu\rho^2 - \rho^4 + \sigma^2 = C. \tag{A6}$$

Here C is a constant that can be determined by the boundary conditions.

The boundary condition (2a) and the conservation law (A6) imply that $\rho(x)$ and $\sigma^2(x)$ tend to constant values as $x \to \pm\infty$. A simple (but not necessarily unique) option compatible with (A2) and (A3), is to assume that $\sigma(x) \to 0$ and $\rho^2(x) \to \mu/2$ as $|x| \to \infty$. The constant C is then identified as $C = \mu^2/4$ and equation (A6) simplifies to

$$\sigma = \pm(\mu/2 - \rho^2). \tag{A7}$$

Here the top and bottom sign correspond to solutions with $\rho^2 \le \mu/2$ and $\rho^2 \ge \mu/2$, respectively.

Making use of the relation (A7), we express θ_x and w from (A4) and (A5):

$$\theta_x = -\frac{\alpha_x}{2} \mp \frac{\sin\alpha}{2\rho}\left(\frac{\mu}{2} + \rho^2\right), \tag{A8}$$

$$w = -\frac{\alpha_x}{2} \pm \frac{\sin\alpha}{2\rho}\left(\frac{\mu}{2} - 3\rho^2\right), \tag{A9}$$

while an equation for ρ is straightforward from (A2):

$$\rho_x \pm (\mu/2 - \rho^2)\cos\alpha = 0. \tag{A10}$$

The general solution of (A10) with the top sign ($\rho^2 \le \mu/2$), is

$$\rho = -\sqrt{\frac{\mu}{2}}\tanh\left[\sqrt{\frac{\mu}{2}}\int\cos\alpha(x)dx\right], \tag{A11}$$

where the indefinite integral incorporates the constant of integration.

Let

$$\alpha(x) = \pi - \arccos\left(\frac{\sin\phi\,\sinh y}{\sqrt{\cosh^2 y + a}}\right), \tag{A12}$$

where

$$y = x\sqrt{\mu/2}\sin\phi,$$

and a, ϕ are two parameters: $-1 < a \le 0$ and $0 \le \phi \le \pi/2$. If we choose the constant of integration so that

$$\int\cos\alpha(x)dx = -\sqrt{\frac{2}{\mu}}\,\mathrm{arctanh}\sqrt{1 + a\,\mathrm{sech}^2 y}, \tag{A13}$$

we will ensure that the argument of tanh in (A11) is negative, hence the right-hand side of (A11) is positive for all x. Thus, equation (A11) with the integral as in (A13) defines the modulus of a solution to the stationary Gross-Pitaevskii equation. The phase of this solution is determined from (A8) while (A9) gives the potential-base function of the equation (3).

Turning to equation (A10) with the bottom sign ($\rho^2 \ge \mu/2$), its general solution reads

$$\rho = \sqrt{\frac{\mu}{2}}\coth\left[\sqrt{\frac{\mu}{2}}\int\cos\alpha(x)dx\right]. \tag{A14}$$

This time, we let

$$\alpha(x) = -\arccos\left(\frac{\sin\phi\sinh y}{\sqrt{\cosh^2 y + a}}\right), \tag{A15}$$

with

$$y = x\sqrt{\mu/2}\sin\phi$$

and two parameters, $a \ge 0$ and $0 \le \phi \le \pi/2$. Choosing the integration constant so that

$$\int\cos\alpha(x)dx = \sqrt{\frac{2}{\mu}}\,\mathrm{arccoth}\sqrt{1 + a\,\mathrm{sech}^2 y}, \tag{A16}$$

we make sure that the argument of coth in (A14) is nowhere negative. Consequently, the expression (A14) with the integral as in (A16), gives the absolute value of another solution the Gross-Pitaevskii equation (3). Its phase $\theta(x)$ and the equation's base function $w(x)$ are straightforward from (A8) and (A9).

The absolute values (A11)+(A13) and (A14)+(A16), can be written in a unified simple form — see equation (8) in the main text. When $a < 0$, the number density $n = \rho^2(x)$ shows a dip at the origin, whereas positive values of a pertain to a hump of the density. The corresponding superfluid velocities $v = \theta_x$ and the potential base functions $w(x)$ also admit a simple expression; see (11) and (10), respectively.

Finally, we can choose $\alpha(x)$ as the negative of expression (A12) or (A15):

$$\alpha = \arccos\left(\frac{\sin\phi\,\sinh y}{\sqrt{\cosh^2 y + a}}\right) - \pi, \quad -1 \le a \le 0,$$

$$\alpha = \arccos\left(\frac{\sin\phi\,\sinh y}{\sqrt{\cosh^2 y + a}}\right), \quad a \ge 0. \tag{A17}$$

The resulting solutions will have the sign of θ_x (and hence the sign of the asymptotic flux) opposite to the one associated with (A12) and (A15).

Acknowledgments

IVB thanks Ricardo Carretero and Boris Malomed for instructive conversations. The work of DAZ and VVK

was supported by the FCT (Portugal) through the grants UID/FIS/00618/2013 and PTDC/FIS-OPT/1918/2012. IVB wishes to acknowledge financial support from the NRF of South Africa (grants UID 85751, 86991, and 87814) and the European Union's Horizon 2020 research and innovation programme under the Marie Skłodowska-Curie grant agreement No 691011.

[1] A. Griffin, *Excitations in a Bose-Condensed liquid* (Cambridge University Press, 1993); L. P. Pitaevskii and S. Stringari, *Bose-Einstein condensation* (Clarendon Press, Oxford, 2003).

[2] see e.g. F. S. Cataliotti, S. Burger, C. Fort, P. Maddaloni, F. Minardi, A. Trombettoni, A. Smerzi, M. Inguscio, Josephson junction arrays with Bose-Einstein condensates, Science **293**, 843 (2001); I. Bloch, Ultracold quantum gases in optical lattices, Nature Phys. **1**, 23 (2005); O. Morsch and M. Oberthaler, Dynamics of Bose-Einstein condensates in optical lattices, Rev. Mod. Phys. **78**, 179 (2006).

[3] A. V. Yulin, Y. V. Bludov, V. V. Konotop, V. Kuzmiak, and M. Salerno, Superfluidity of Bose-Einstein condensates in toroidal traps with nonlinear lattices, Phys. Rev. A, **84**, 063638 (2011); A. V. Yulin, Yu. V. Bludov, V. V. Konotop, V. Kuzmiak, and M. Salerno, Superfluidity breakdown of periodic matter waves in quasi-one-dimensional annular traps via resonant scattering with moving defects, Phys. Rev. A, **87**, 033625 (2013).

[4] H. P. Büchler, V. B. Geshkenbein, and G. Blatter, Superfluidity versus Bloch oscillations in confined atomic gases, Phys. Rev Lett. **87**, 100403 (2001); G. E. Astrakharchik and L. P. Pitaevskii, Motion of a heavy impurity through a Bose-Einstein condensate, Phys. Rev. A **70**, 013608 (2004); A. Polkovnikov, E. Altman, E. Demler, B. Halperin, and M. D. Lukin, Decay of superfluid currents in a moving system of strongly interacting bosons, Phys. Rev. A **71**, 063613 (2005); A. G. Sykes, M. J. Davis and D. C. Roberts, Drag force on an impurity below the superfluid critical velocity in a quasi-one-dimensional Bose-Einstein condensate, Phys. Rev. Lett. **103**, 085302 (2009).

[5] A. Ramanathan, K. C. Wright, S. R. Muniz, M. Zelan, W. T. Hill III, C. J. Lobb, K. Helmerson, W. D. Phillips, and G. K. Campbell, Superflow in a toroidal Bose-Einstein condensate: An atom circuit with a tunable weak link, Phys. Rev. Lett. **106**, 130401 (2011).

[6] V. A. Brazhnyi, V. V. Konotop, V. M. Pérez-García, and H. Ott, Dissipation-induced coherent structures in Bose-Einstein condensates, Phys. Rev. Lett. **102**, 144101 (2009); D. A. Zezyulin, V. V. Konotop, G. Barontini, and H. Ott, Macroscopic Zeno effect and stationary flows in fonlinear waveguides with localized dissipation, Phys. Rev. Lett. **109**, 020405 (2012); D. A. Zezyulin and V. V. Konotop, Stationary vortex flows and macroscopic Zeno effect in Bose-Einstein condensates with localized dissipation, Rom. Rep. Phys. **67**, 223 (2015).

[7] G. Barontini, R. Labouvie, F. Stubenrauch, A. Vogler, V. Guarrera, and H. Ott, Controlling the dynamics of an open many-body quantum system with localized dissipation, Phys. Rev. Lett. **110**, 035302 (2013).

[8] V. S. Shchesnovich and V. V. Konotop, Control of a Bose-Einstein condensate by dissipation: Nonlinear Zeno effect, Phys. Rev. A **81**, 053611 (2010).

[9] A. Kavokin, G. Malpuech, F. P. Laussy, Polariton laser and polariton superfluidity in microcavities, Phys. Lett. A **306**, 187 (2003); E. Cancellieri, F. M. Marchetti, M. H. Szymańska, and C. Tejedor, Superflow of resonantly driven polaritons against a defect, Phys. Rev. B, **82**, 224512 (2010); M. Wouters and I. Carusotto, Superfluidity and critical velocities in nonequilibrium Bose-Einstein condensates, Phys. Rev. Lett. **105**, 020602 (2010); A. Amo, S. Pigeon, D. Sanvitto, V. G. Sala, R. Hivet, I Carusotto, F. Pisanello, G. Leménager, R. Houdré, E. Giacobino, C. Ciuti, A. Bramati, Polariton superfluids reveal quantum hydrodynamic solitons, Science **332**, 1167 (2011).

[10] J. G. Muga, J. P. Palao, B. Navarro, and I. L. Egusquiza, Complex absorbing potentials, Phys. Rep. **395**, 357 (2004).

[11] V. V. Konotop, J. Yang, and D. A. Zezyulin, Nonlinear waves in $\mathcal{PT}$-symmetric systems, Rev. Mod. Phys. **88**, 035002 (2016).

[12] C. M. Bender and S. Boettcher, Real spectra in non-Hermitian Hamiltonians having $\mathcal{PT}$ symmetry, Phys. Rev. Lett. **80**, 5243 (1998).

[13] H. Cartarius and G. Wunner, Model of a PT-symmetric Bose-Einstein condensate in a δ-function double-well potential, Phys. Rev. A **86**, 013612 (2012); E.-M. Graefe, Stationary states of a PT symmetric two-mode Bose-Einstein condensate, J. Phys. A. **45**, 444015 (2012); A. S. Rodrigues, K. Li, V. Achilleos, P. G. Kevrekidis, D. J. Frantzeskakis, and C. M. Bender, PT-symmetric double-well potentials revisited: bifurcations, stability and dynamics Rom. Rep. Phys. **65**, 5 (2013); D. Dast, D. Haag, and H. Cartarius, Eigenvalue structure of a Bose-Einstein condensate in a $\mathcal{PT}$-symmetric double well, J. Phys. A. **46** 375301 (2013); Y. V. Kartashov, V. V. Konotop, and D. A. Zezyulin, $\mathcal{CPT}$-symmetric spin-orbit-coupled condensate, EPL (Europhysics Letters) **107**, 50002 (2014).

[14] D. Haag, D. Dast, H. Cartarius, and G. Wunner, $\mathcal{PT}$-symmetric currents of a Bose-Einstein condensate in a triple well, Phys. Rev. A **92**, 053627 (2015).

[15] I. V. Barashenkov, D. A. Zezyulin, and V. V. Konotop, Jamming anomaly in $\mathcal{PT}$-symmetric systems, New J. Phys. **18**, 075015 (2016).

[16] D. A. Zezyulin and V. V. Konotop, Nonlinear currents in a ring-shaped waveguide with balanced gain and dissipation, Phys. Rev. A **94** 043853 (2016).

[17] M. Wadati, Construction of Parity-Time symmetric potential through the Soliton Theory, J. Phys. Soc. Jpn. **77**, 074005 (2008).

[18] E. N. Tsoy, I. M. Allayarov, and F. Kh. Abdullaev, Stable localized modes in asymmetric waveguides with gain and loss, Opt. Lett. **39**, 4215 (2014).

[19] V. V. Konotop and D. A. Zezyulin, Families of stationary modes in complex potentials, Opt. Lett. **39**, 5535 (2014).

[20] J. Yang, Symmetry breaking of solitons in one-dimensional parity-time-symmetric optical potentials,

Opt. Lett. **39**, 5547 (2014); S. Nixon, J. Yang, Bifurcation of soliton families from linear modes in non-PT-symmetric complex potentials, Stud. Appl. Math. **136**, 459 (2016).

[21] K. G. Makris, Z. H. Musslimani, D. N. Christodoulides, and S. Rotter, Constant-intensity waves and their modulation instability in non-Hermitian potentials, Nat. Commun. **6**, 7257 (2015).

[22] I. V. Barashenkov, D. A. Zezyulin, and V. V. Konotop, Exactly solvable Wadati potentials in the $\mathcal{PT}$-symmetric Gross-Pitaevskii equation. In: Non-Hermitian Hamiltonians in Quantum Physics. Selected Contributions from the 15th International Conference on Non-Hermitian Hamiltonians in Quantum Physics, Palermo, Italy, 18-23 May 2015. F. Bagarello, R. Passante, and C. Trapani: Editors. Springer Proceedings in Physics, vol. 184. Springer International Publishing, Switzerland (2016), pp 143-155. DOI: 10.1007/978-3-319-31356-6_9

[23] Z. Ahmed, Real and complex discrete eigenvalues in an exactly solvable one-dimensional complex $\mathcal{PT}$-invariant potential, Phys. Lett. A **282**, 343 (2001); Addendum to: Real and complex discrete eigenvalues in an exactly solvable one-dimensional complex $\mathcal{PT}$-invariant potential *ibidem* **287**, 295 (2001).

[24] Z. Shi, X. Jiang, X. Zhu, and H. Li, Bright spatial solitons in defocusing Kerr media with $\mathcal{PT}$-symmetric potentials, Phys. Rev. A **84**, 053855 (2011).

[25] Y.-J. He and B. A. Malomed. Spatial Solitons in Parity-Time-Symmetric Photonic Lattices: Recent Theoretical Results. In: Spontaneous Symmetry Breaking, Self-Trapping, and Josephson Oscillations. B. A. Malomed: Editor. Progress in Optical Science and Photonics, vol. 1. Springer-Verlag Berlin Heidelberg (2013), pp. 125-148. DOI: 10.1007/10091_2012_24